Crystal structure and thermoelectric properties of chimney–ladder compounds in the Ru2Si3–Mn4Si7 pseudobinary system

AUTHOR(S):

Okamoto, Norihiko L.; Koyama, Tatsuya; Kishida, Kyosuke; Tanaka, Katsushi; Inui, Haruyuki

CITATION:

Okamoto, Norihiko L. ...[et al]. Crystal structure and thermoelectric properties of chimney–ladder compounds in the Ru2Si3–Mn4Si7 pseudobinary system. Acta Materialia 2009, 57(17): 5036-5045

ISSUE DATE:

2009-10

URL:

http://hdl.handle.net/2433/123373

Crystal structure and thermoelectric properties of chimney-ladder compounds in the Ru_2Si_3-Mn_4Si_7 pseudobinary system

By Norihiko L. Okamoto*, Tatsuya Koyama, Kyosuke Kishida, Katsushi Tanaka and Haruyuki Inui

Department of Materials Science and Engineering, Kyoto University

Sakyo-ku, Kyoto 606-8501, Japan

Abstract

Phase relationships of manganese-substituted ruthenium sesquisilicide alloys have been investigated by using x-ray powder diffraction, scanning and transmission electron microscopy. A series of chimney-ladder phases $Ru_{1-x}Mn_xSi_y$ ($0.14 \leq x \leq 0.97$, $1.584 \leq y \leq 1.741$) are formed over a wide compositional range between Ru_2Si_3 and Mn_4Si_7. The compositions of these actually formed chimney-ladder compounds are deviated slightly from the composition line connecting Ru_2Si_3 and Mn_4Si_7, which corresponds to the ideal composition line satisfying the VEC (valence electron counting)=14 rule. The occurrence of the compositional deviation is discussed in terms of the VEC rule and the atomic packing. The thermoelectric properties of the directionally solidified $Ru_{1-x}Mn_xSi_y$ alloys ($0.55 \leq x \leq 0.90$) have also been investigated as a function of the Mn content and temperature. The dimensionless figure-of-merit (ZT) for the alloys with high Mn contents ($x \geq 0.75$) increases with the increase in the Mn content. The ZT value for the crystal with $x = 0.90$ is as high as 0.76 at 874 K.

Keywords: transition metal silicide; transmission electron microscopy (TEM); x-ray diffraction (XRD); directional solidification; thermal conductivity

Corresponding author (*):

Norihiko L. Okamoto

Assistant Professor

Department of Materials Science and Engineering, Kyoto University

Sakyo-ku, Kyoto 606-8501, Japan

TEL: +81-75-753-5481

FAX: +81-75-753-5461

E-mail: n.okamoto@at4.ecs.kyoto-u.ac.jp

1. Introduction

Semiconducting ruthenium sesquisilicide (Ru_2Si_3) has two allotropic phases separated by a reversible and diffusionless phase transformation approximately at 1300K [1,2]. The high-temperature (HT) phase possesses the tetragonal Ru_2Sn_3-type structure, which is known as one of the chimney-ladder structures, whereas the low-temperature (LT) phase possesses the orthorhombic Ru_2Si_3-type structure [1,3]. Some of the family of compounds with the chimney-ladder structures, including high manganese silicides (Mn_4Si_7 [4], $Mn_{11}Si_{19}$ [5], $Mn_{15}Si_{26}$ [6] and so forth), are known to exhibit a high Seebeck coefficient and low thermal conductivity simultaneously so that they have been investigated as a candidate for thermoelectric materials [7-10] because the thermoelectric performance is evaluated with the dimensionless figure-of-merit, $ZT = \alpha^2 T/(\rho \cdot \lambda)$, where α, ρ, λ and T stand for Seebeck coefficient, electrical resistivity, thermal conductivity and temperature, respectively. The chimney-ladder compounds expressed with the general chemical formula of M_nX_{2n-m} (M: transition metal element, X: group 13 or 14 element, n, m: integers) possess a particular tetragonal crystal structure, in which the unit cell consists of M (Ru) subcell with the atomic arrangement of the β-Sn type (chimney) and X (Si) sucell with the atomic arrangement of a coupled helices (ladders) with both the chimney and ladder being aligned along the c-axis of the tetragonal unit cell (Fig. 1) [1,11,12]. Therefore, the c-axis dimension (c) of the unit cell of the chimney-ladder structure composed of nM subcells and mX subcells is in general expressed with the least common multiple of the c-axis dimensions (c_M and c_X) of these two subcells; $c = nc_M = mc_X$. HT Ru_2Si_3 possesses the simplest type of the chimney-ladder structure with the unit cell (with $n = 2$ and $m = 1$) expressed with $c = 2c_M = c_X$. Then, the X/M atomic ratio of the chimney-ladder compound M_nX_{2n-m} is related with the c_X/c_M ratio, as follows [11,13];

$$\frac{X}{M} = \frac{2n-m}{n} = 2 - \left(\frac{c_X}{c_M}\right)^{-1}. \quad (1)$$

Since the chimney-ladder compounds are known to be electron compounds following an valence electron counting (VEC) rule [11,14-16], the X/M ratio of a particular binary chimney-ladder compound such as Ru_2Si_3 is expected to be controlled by substituting some of M atoms with another transition metal element whose number of valence electrons is different from that for M atoms. For example, if some of Ru atoms belonging to group 8 of the periodic table (the group numbers in the present paper are all referred to the convention of International Union of Pure and Applied Chemistry (IUPAC)) in Ru_2Si_3 is substituted with Re atoms belonging to group 7, the Si/(Ru+Re) ratio should change from 3/2 to stabilize the crystal structure, i.e., it should increase to compensate the decreased valence electrons.

In fact, we have recently found out that substitutions of Ru in Ru_2Si_3 with Re stabilize the HT phase with the chimney-ladder structure to appear at low temperatures so that a series of chimney-ladder phases, $Ru_{1-x}Re_xSi_y$ are formed over a wide composition range [13,17]. Of interest to note is that the X/M values for these chimney-ladder phases deviate from the ideal values expected from the VEC=14 rule. The X/M values for alloys with low Re contents (x < 0.5) is larger than the ideal values (i.e., VEC > 14) while those for alloys with high Re contents (x > 0.5) is smaller than the ideal values (i.e., VEC < 14), with the interception occurring at about x = 0.5. Hence, these alloys exhibit n- and p-type semiconducting behaviors at low and high Re concentrations, respectively. Since the extent of compositional deviation from the ideal VEC=14 values is considered to correspond to the carrier concentration, the absolute values of both Seebeck coefficient and electrical resistivity increase as the extent of the deviation from the VEC=14 rule increases, i.e., as the alloy composition deviates from that corresponding to the p-n transition (x = 0.5) [18]. The

occurrence of the compositional deviation from the ideal values satisfying the VEC=14 rule is considered to be closely related to the changes in atomic packing caused by the difference in atomic radius between Ru (0.134 nm) and Re (0.138 nm) [18]. These chimney-ladder phases can exist when the values of atomic packing factor are in a certain range and that these phases are destabilized once atomic packing becomes out of the range. Then, these chimney-ladder phases tend to take X/M ratios within the range of atomic packing factor, which is different from that the VEC=14 rule dictates. Thus, the compositional deviation from the ideal values satisfying the VEC=14 rule is considered to be controlled by alloying additions not only through the difference in the number of valence electrons between Ru and the substitutional element but also through the difference in atomic radius between the two. In this perspective, it is very interesting to investigate how the compositional deviation from the ideal values occurs when some of Ru in Ru_2Si_3 is substituted with Mn, since Mn belongs to group 7 as Re does and the atomic radius of Mn (0.126 nm) is considerably smaller than that of Ru. In the case of Mn substitutions, the composition range in which a series of chimney-ladder phases, $Ru_{1-x}Mn_xSi_y$ are formed is expected to be very large (almost in the entire pseudobinary composition range) because of the existence of Mn_4Si_7, which is known to possess the chimney-ladder structure with $n = 4$ and $m = 1$ [12].

In the present study, we investigate the phase relationships and crystal structures in Mn-substituted ruthenium sesquisilicide alloys by x-ray powder diffraction, scanning electron microscopy (SEM) and transmission electron microscopy (TEM). We also investigate the thermoelectric properties of directionally solidified crystals of the chimney-ladder compounds in the Ru-Mn-Si system as a function of the Mn content and temperature with an expectation of further enhancing the thermoelectric properties.

2. Experimental procedures

Polycrystalline specimens with nominal compositions of $Ru_{1-x}Mn_xSi_{1.5}$ (x = 0.05, 0.20, 0.40, 0.60, and 0.80) and $Ru_{1-x}Mn_xSi_{1.75}$ (x = 0.20, 0.40, 0.60, and 0.80) were prepared by arc-melting elemental Ru (3N-grade), Mn (4N-grade), semiconductor-grade Si under an Ar gas flow. Microstructures of the as-grown samples were examined by SEM and TEM. Chemical compositions for selected regions of interest were estimated by energy dispersive x-ray spectroscopy (EDS) in both SEM and TEM. Samples for TEM observations were prepared by mechanical polishing, dimple grinding and finally Ar-ion milling for electron transparency. After determining the stable composition range for the chimney-ladder phases in the Ru-Mn-Si system with the use of arc-melted alloys, In order to produce specimens for measurements of thermoelectric properties, directional solidification was made for some $Ru_{1-x}Mn_xSi_y$ alloys (x = 0.50, 0.55, 0.75, 0.85 and 0.90; the value of y is determined based on investigation of the phase relationship as described in the Section 3.1) by the Czochralski method (x = 0.50, 0.55 and 0.75) and by the optical floating zone method (x = 0.85 and 0.90) at a growth rate of 5 mm/h under an Ar gas flow.

Specimens with a rectangular parallelepiped shape having approximate dimensions of 2×2×7 mm^3 were cut from these directionally solidified ingots by electric discharge machining and were used for measurements of Seebeck coefficient and electrical resistivity. Seebeck coefficient and electrical resistivity were measured in the temperature range from 323 to 1023 K by the static dc and four-probe methods, respectively, with our ZEM-2 apparatus (ULVAC, Japan). Thermal conductivity was estimated from the values of thermal diffusivity and specific heat measured for thin-disc samples with a diameter of 8 mm and a thickness of 1 mm in the temperature range from room temperature to 1073 K by the laser flash method with our TC-7000 apparatus (ULVAC, Japan).

3. Results

3.1 Phase equilibria and structural variation in the chimney-ladder phases

3.1.1. SEM microstructures

Figs. 2(a)-(d) and Figs. 2(f)-(i) show SEM backscattered electron images (BEIs) of as-arcmelted samples with nominal alloy compositions of $Ru_{1-x}Mn_xSi_{1.5}$ and $Ru_{1-x}Mn_xSi_{1.75}$ (x = 0.20, 0.40, 0.60, and 0.80), respectively. Two phases are identified for all the samples with the major phase being the (Ru,Mn)Si_y sesquisilicide phase. While the second phase observed for $Ru_{1-x}Mn_xSi_{1.5}$ alloys is the (Ru,Mn)Si monosilicide phase (as indicated by white arrows in Figs. 2(a)-(d)), it is the Si phase for $Ru_{1-x}Mn_xSi_{1.75}$ alloys (as indicated by black arrows in Figs. 2(f)-(i)). The volume fraction of the (Ru,Mn)Si monosilicide second phase increases as the Mn content in $Ru_{1-x}Mn_xSi_{1.5}$ alloys increases, while the opposite is true for the Si second phase in $Ru_{1-x}Mn_xSi_{1.75}$ alloys, indicating that the Si content in the sesquisilicide phase increases as the Mn content increases. The major (Ru,Mn)Si_y sesquisilicide phase is always accompanied by contrast variation within the region. EDS analysis in a SEM has revealed that the contrast variation corresponds to compositional variation in the (Ru,Mn)Si_y sesquisilicide phase, as observed previously for the chimney-ladder phases in the Ru-Re-Si ternary system [13,17,18]. Thus, a range of composition is indicated for the (Ru,Mn)Si_y sesquisilicide phase in the ternary phase diagrams of Figs. 2(e) and (j) for each of $Ru_{1-x}Mn_xSi_{1.5}$ and $Ru_{1-x}Mn_xSi_{1.75}$ alloys, respectively. The extent of the compositional variation in the (Ru,Mn)Si_y sesquisilicide phase is much larger than that previously observed in the (Ru,Re)Si_y sesquisilicide phase [13,17,18] and is hardly changed significantly by annealing at 1373 K for 96 h.

3.1.2. X-ray diffraction analysis

X-ray diffraction patterns obtained for $Ru_{1-x}Mn_xSi_{1.5}$ alloys with x = 0.05, 0.20, 0.40, 0.60 and 0.80 are shown in Fig. 3 in the 2θ range from 20 to 80 degrees, together with those calculated for HT-Ru_2Si_3 [19] and B20-type RuSi monosilicide [20]. While the (Ru,Mn)Si_y sesquisilicide phase is exclusively observed in the specimen with x = 0.05, both the (Ru,Mn)Si_y sesquisilicide and monosilicide phases observed for other specimens. When judged from the relative intensities, the volume fraction of the monosilicide phase increases with the increase in the Mn content, being consistent with the SEM-EDX results described in the previous section.

The values of lattice constants (of the metal subcell) a_M and c_M of the tetragonal (Ru,Mn)Si_y sesquisilicide are estimated from the X-ray diffraction data (Fig. 3) and are plotted in Fig. 4(a) as a function of the nominal Mn content, together with those for Mn_4Si_7 [21]. The value of c_M monotonically decreases with the increase in the Mn content, while that of a_M increases with the increase in the Mn content for smaller Mn contents, followed by the decrease for larger Mn contents. As a result, the cell volume of the M subcell v_M ($=a_M^2 \times c_M$) decreases with the increase in the Mn content, as shown in Fig. 4(b).

3.1.3. TEM analysis

Fig. 5(a) shows a TEM bright-field image of a sample with the nominal composition of $Ru_{0.40}Mn_{0.60}Si_{1.75}$. A grain of the (Ru,Mn)$Si_y$ sesquisilicide phase is located next to a grain of the Si phase. TEM-EDX analysis revealed that the Mn content in the sesquisilicide phase decreases as the distance from the Si grain increases, being consistent with the SEM-EDX analysis shown in Figs. 2(h) and (j). Selected-area electron diffraction (SAED) patterns (Figs. 5(b)-(d)) taken from the positions in the sesquisilicide phase denoted ‘b’, ‘c’ and ‘d’ in Fig.

5(a) all exhibit characteristics of the chimney-ladder structure consisting of diffraction spots from the M subcell and those from the Si subcell. This indicates that the HT-phase of Ru_2Si_3 with the chimney-ladder structure is stabilized by the substitution of Ru with Mn so as to appear even at low temperatures. All the SAED patterns of Fig. 5 are indexed as those with the $[120]_M$ incidence when referred to the M subcell but the spacing of satellite spots from the Si subcell in the 00*l* systematic row increases as the Mn content decreases, i.e., as the distance from the Si grain increases. This indicates that some different chimney-ladder phases with different Si subcell sizes along the *c*-axis are formed within a grain of the sesquisilicide phase, preserving the crystal orientation, which is basically determined by that of the M subcell. Typical examples of the 00*l* systematic row in the SAED pattern taken along the [120] direction of chimney-ladder phases from various specimens of $Ru_{1-x}Mn_xSi_{1.5}$ and $Ru_{1-x}Mn_xSi_{1.75}$ alloys (with $0.20 \leq x \leq 0.80$) are shown in Fig. 6 in the increasing order of the Mn/M ratio, which is estimated by TEM-EDX analysis. The c_{Si}/c_M ratios of these chimney-ladder phases are determined from the SAED patterns with the following equation,

$$\frac{c_{Si}}{c_M} = \frac{R_{002M}}{2(R_{001Si})}, \qquad (2)$$

where R_{002M} and R_{001Si} are the distances between the transmitted spot and 002_M and 001_{Si} diffraction spots, respectively (Fig. 6) [12,13]. Then, the Si/M atomic ratios in the corresponding chimney-ladder phases are determined with Eq. (1). The c_{Si}/c_M and Si/M ratios determined from these SAED patterns with Eqs. (1) and (2) are shown in Fig. 6 together with the Mn/M ratio determined by TEM-EDX analysis. The value of the Si/M ratio increases as the value of the Mn/M ratio increases, being consistent with the results of SEM-EDX analysis (Fig. 2). Chimney-ladder phases are thus confirmed to exist in a wide composition range of $0.14 \leq x \leq 0.97$ and $1.584 \leq y \leq 1.741$ when expressed in the form of $Ru_{1-x}Mn_xSi_y$. The sesquisiliside phase with the Mn content less than $x = 0.14$ possesses an additional

superstructure along the *a*-axis of a chimney-ladder structure. The details of crystal structure refinement for the phase appearing for alloys with less Mn contents will be published elsewhere [22].

The values of the Si/M ratio (y) thus obtained for chimney-ladder phases are plotted in Fig. 7 as a function of the Mn content (x in the formula of $Ru_{1-x}Mn_xSi_y$), together with the similar plot previously obtained for chimney-ladder phases in the Ru-Re-Si ternary system [13,18]. The values of the Si/M ratio for most chimney-ladder phases in the Ru-Mn-Si system are larger than those expected from the VEC=14 rule, and they become identical to or a little smaller than those expected from the VEC=14 rule only at the high Mn contents ($x \geq$ ~0.9). This is in contrast to what is observed for chimney-ladder phases in the Ru-Re-Si ternary system, in which the interception of the two occurs at an intermediate Re content around x=0.5. The reasons for this will be discussed later.

Phase relationships among sesquisilicide, monosilicide and Si phases are described in Fig. 8 based on the results obtained in the present study. A series of chimney-ladder phase exist as the sesquisilicide phase in a wide range of the Mn content ($0.14 \leq x \leq 0.97$). Sesquisilicide-monosilicide as well as sesquisilicide-Si two-phase regions are observed in wide composition ranges.

3.2. Microstructure and thermoelectric properties of directionally solidified alloys

3.2.1. Microstructures

Five different nominal compositions as tabulated in Table 1 were selected for crystal growth by directional solidification based on the result described in the previous section (Fig. 8). Contrary to the case of chimney-ladder compounds in the Ru-Re-Si system [18], it was impossible to obtain single crystals of chimney-ladder compounds in the Ru-Mn-Si system.

However, crystal orientation analysis by the x-ray back reflection Laue method has revealed that crystals grow preferentially along the *c*-axis of the tetragonal chimney-ladder phases. Microstructures observed in longitudinal sections of the grown crystals are depicted in Fig. 9, in which the growth direction is set in parallel to the horizontal edge of figures. All the crystals exhibit virtually a sesquisilicide single-phase microstructure. The sesquisilicide phase in directionally solidified alloys also exhibits compositional variation due to the formation of many different chimney-ladder phases, as observed in the as-arcmelted samples (Fig. 2). The compositional variations observed in these directionally solidified alloys are described with the intensity histograms in the right-hand side of Fig. 9, which are constructed from the corresponding grey-scale SEM-BEIs on the assumption that the intensity decreases linearly with the increase in the Mn content. Although the compositional ranges for the sesquisilicide phase of the different alloys overlap with each other, the peak Mn content increases with the increase in the nominal Mn content.

3.2.2. Thermoelectric properties

Thermoelectric properties of the directionally solidified $Ru_{1-x}Mn_xSi_y$ alloys were evaluated along the growth direction. Values of Seebeck coefficient for these alloys are plotted in Fig. 10(a) as a function of temperature. The alloys with x = 0.50 and 0.55 exhibit negative values in the whole temperature range investigated whereas those with x = 0.75, 0.85 and 0.90 exhibit positive values. The absolute values of Seebeck coefficient for the alloy with x = 0.55 are considerably smaller than those for the alloy with x = 0.50. The value for the alloy with x = 0.75 is slightly smaller than those with x = 0.85 and 0.90 at room temperature, and the difference in the values increases with the increase in temperature. Values of electrical resistivity for directionally solidified alloys are plotted in Fig. 10(b) as a

function of temperature. While the values of electrical resistivity for the alloy with x = 0.75 decrease with the increase in temperature, those for the alloys with x = 0.50, 0.85 and 0.90 increase with increasing temperature, which is a characteristic of degenerated semiconductors. For the alloy with x = 0.55, the values of electrical resistivity slightly increase with the increase in temperature up to 600 K, followed by a decrease at higher temperatures. The values of electrical resistivity for the alloys with x = 0.50, 0.85 and 0.90 are smaller than those with x = 0.55 and 0.75 by an order of magnitude. Values of thermal conductivity for directionally solidified alloys with x = 0.85 and 0.90 are plotted in Fig. 10(c) as a function of temperature. The values of thermal conductivity for both alloys increase with the increase in temperature, in particular at high temperatures above 800 K.

Values of thermoelectric power factor and dimensionless figure of merit (ZT) calculated with the obtained values of electrical resistivity, Seebeck coefficient and thermal conductivity are plotted respectively in Figs. 10(d) and (e) as a function of temperature, together with the similar plots for the best alloy in the Ru-Re-Si ternary system [18]. Whereas the values of power factor for the alloys with x = 0.55 and 0.75 are considerably low, those for the alloys with x = 0.50, 0.85 and 0.90 are relatively high. The highest value of power factor (1.5×10^{-3} W/mK^2) is obtained for the alloy with x = 0.90 at 780 K. The ZT values for the alloys with x = 0.85 and 0.90 increase with the increase in temperature up to 850 K, followed by a rather rapid decrease at high temperatures. The highest ZT value for the alloy with x = 0.90 is as high as 0.76 at 874 K, which is much higher than that obtained for the $Ru_{0.40}Re_{0.60}Si_{1.663}$ alloy (ZT=0.56 at 973 K) [18].

4. Discussion

4.1. Crystal structure: VEC=14 rule and atomic packing

As described above, chimney-ladder compounds in the Ru-Mn-Si system also behave as electronic compounds, following the VEC=14 rule [11,14-16]. However, these chimney-ladder compounds in the Ru-Mn-Si system do not precisely obey the VEC=14 rule, as shown in Fig. 11(a) where the VEC values of the experimentally observed chimney-ladder phases are plotted as a function of the Mn content. The VEC values for the chimney-ladder phases with compositions close to Mn_4Si_7 ($\sim 0.9 \leq x \leq 0.97$) are slightly smaller than 14. This is reasonable in view of the fact that the chimney-ladder phase in the Mn-Si binary system is reported to have a solid solubility range from Mn_4Si_7 (Si/M=1.75) to $Mn_{11}Si_{19}$ (Si/M=1.727) so as to form a series of compounds with VEC<14 [5,21]. On the other hand, the VEC values for the chimney-ladder compounds with compositions of $0.14 \leq x \leq \sim 0.9$ are larger than 14. Upon alloying Mn_4Si_7 with Ru, the value of the Si/M ratio should decrease with the increase in the Ru content so as to maintain VEC=14. The larger VEC values of these chimney-ladder compounds indicate that Si atoms exist in their lattices in excess of what is expected from the VEC rule. The amount of excess Si atoms (i.e., the VEC value) in $(Ru,Mn)Si_y$ compounds increases with the increase in the Ru content up to $x = \sim 0.5$ (Fig. 11(a)). Of interest to note is that the cell volume of the M subcell v_M ($=a_M^2 \times c_M$) increases with the increase in the Ru content also up to $x = \sim 0.5$ (Fig. 4(b)). These indicate that these excess Si atoms are introduced to maintain the atomic packing (defined as the ratio of the volume of atoms located in the unit metal subcell to the volume of the unit metal subcell) of the chimney-ladder structure, as observed in the Ru-Re-Si system [18]. The values of the atomic packing factor calculated for actual compositions of the experimentally observed chimney-ladder phases are plotted as a function of the Mn content, together with those estimated for the corresponding VEC=14 compositions. Goldschmidt radii (0.134, 0.126 and 0.117 nm respectively for Ru, Mn and Si) are used in the calculation. Indeed, the values of

the atomic packing factor for the experimentally determined compositions vary with the composition less significantly than those estimated for the corresponding VEC=14 compositions, indicating that the chimney-ladder phases are stabilized by maintaining the atomic packing factor in a certain range. Thus, the VEC value of (Ru,Mn)Si_y chimney-ladder compounds increases with the increase in the Ru content (up to x = ~0.5) due to the increased amount of excess Si atoms, which are introduced in the lattice to maintain the atomic packing factor in a certain range in the circumstance of the increase in the cell volume of the M subcell.

Upon further alloying Mn_4Si_7 with Ru ($0.14 \leq x \leq \sim 0.5$), the VEC values of the experimentally observed chimney-ladder phases do not significantly change with the Ru content. In the alloy composition range, the change in the cell volume of the M subcell is not so significant when compared to that in the alloy composition range of $\sim 0.5 \leq x < 1$) (Fig. 4(b)). This indicates that the amount of excess Si atoms to be introduced to maintain the atomic packing factor may not be so large in the alloy composition range. These may be due to the fact that the deviation of VEC values of these chimney-ladder compounds from the ideal value (VEC=14) are in their upper limit and that the introduction of more excess Si atoms in their lattices may destabilize the chimney-ladder crystal structure.

4.2. Thermoelectric properties and deviation from VEC=14

For the chimney-ladder compounds ($Ru_{1-x}Re_xSi_y$) in the Ru-Re-Si system, the Si/M ratio also deviates from that expected from the VEC=14 rules, as shown in Fig. 7 [13,18]. The Si/M values are larger than those expected from the VEC=14 rule for smaller x values (smaller Re contents), while the opposite is true for larger x values (larger Re contents) with the interception occurring at the x value around 0.5. This Re content observed for the

interception (x~0.5) coincides with that at which the n-p transition in the conduction type is observed (n-type for VEC>14 and p-type for VEC<14). If this is true also for the chimney-ladder compounds ($Ru_{1-x}Mn_xSi_y$) in the Ru-Mn-Si system, the n-p transition should occur at the x value around 0.9 (Figs. 7 and 11(a)). However, the measurements of Seebeck coefficient have revealed that the n-p transition for $Ru_{1-x}Mn_xSi_y$ occurs a composition between x = 0.55 and 0.75 in $Ru_{1-x}Mn_xSi_y$, as shown in Fig. 10(a). We suspect that this inconsistency in the Mn content in $Ru_{1-x}Mn_xSi_y$ compounds may come from a combined effect from their electronic structure and compositional variation. The band calculation of the electron structures for HT-Ru_2Si_3 and Mn_4Si_7 has indicated that the curvature of the highest valence band is much larger than that of the lowest conduction band at the gamma point in the Brillouin zone, suggesting that the carrier mobility for holes is much larger than that for electrons [19,23]. Then, if a specimen contains both p- (Mn-rich) and n-type (Mn-poor) chimney-ladder phases, the sign of Seebeck coefficient would be positive because of the dominance of the hole contribution as indicated below [24].

$$\alpha = \frac{\alpha_h n_h \mu_h + \alpha_e n_e \mu_e}{n_h \mu_h + n_e \mu_e}, \qquad (3)$$

where n and μ stand for the carrier concentration and carrier mobility, respectively, and subscripts h and e denote hole and electron, respectively. As described in 3.1.1 section, the extent of the compositional variation observed in each specimen consisting of a series of chimney-ladder compounds is much larger in (Ru,Mn)Si_y alloys than in (Ru,Re)Si_y alloys. This indicates that there is a high chance for many of (Ru,Mn)Si_y alloys (especially in the Mn-rich compositions) to contain some chimney-ladder compounds of the p-type so as to exhibit a p-type behavior, even though the major volume fraction is occupied by those of the n-type. Then, it is reasonable that the Mn content at which the p-n transition is observed is apparently shifted towards the lower Mn content from that expected from the Si/M relation

corresponding to the interception.

The considerably small values and of Seebeck coefficient and power factor for the alloy with x = 0.55 and 0.75 are then reasonably considered to be due to the cancelling out of the contributions from the n- and p-type compounds. On the other hand, once an alloy consists of either of n- or p-type compounds, the values of power factor become high as observed in alloys with x = 0.50 (n-type) and x = 0.85 and 0.90 (p-type). The alloy with x = 0.90 exhibits the highest value of power factor (1.5×10^{-3} W/mK^2), which is even higher than the highest value obtained for the chimney-ladder compound in the Ru-Re-Si system ($Ru_{0.27}Re_{0.73}Si_{1.671}$: 0.9×10^{-3} W/mK^2) [18]. The ZT value (0.76 at 874 K) for the alloy with x = 0.90 is also higher than the highest value (0.49 at 950 K) obtained for the chimney-ladder compound in the Ru-Re-Si system ($Ru_{0.40}Re_{0.60}Si_{1.663}$) [18].

5. Conclusions

(1) The HT-Ru_2Si_3 phase with the chimney-ladder structure is stabilized to appear at low temperatures by the substitution of Ru with Mn to form a series of chimney-ladder compounds $Ru_{1-x}Mn_xSi_y$ over a wide composition range between Ru_2Si_3 and Mn_4Si_7.

(2) The compositions of these actually formed chimney-ladder compounds are deviated slightly from the composition line connecting Ru_2Si_3 and Mn_4Si_7, which corresponds to the ideal composition line satisfying the VEC=14 rule.

(3) The occurrence of the compositional deviation is explained in terms of the valence electron counting rule and atomic packing. The VEC value of (Ru,Mn)Si_y chimney-ladder compounds increases with the increase in the Ru content (up to x = ~0.5) due to the increased amount of excess Si atoms, which are introduced in the lattice to maintain the atomic packing factor in a certain range in the circumstance of the increase in the cell volume of the M

subcell. On the other hand, the VEC values do not significantly change with the Ru content ($0.14 \leq x \leq \sim 0.5$) because of the less significant change in the cell volume of the M subcell.

(4) The $Ru_{1-x}Mn_xSi_y$ chimney-ladder phases exhibit n- and p-type semiconducting behaviors respectively at low and high Mn concentrations, at which the X/M values are respectively larger and smaller than those expected from the VEC=14 rule. The carrier mobility for holes is expected to be much larger than that for electrons when judged from the occurrence of the p-n transition at a composition between $x = 0.55$ and 0.75.

(5) The values of thermoelectric power factor and *ZT* for the alloys with high Mn contents ($x > 0.75$) increase with the increase in the Mn content. The *ZT* value for the alloy with $x = 0.90$ is as high as 0.76 at 880 K, which is higher than the highest value obtained for the ternary alloys in the Ru-Re-Si system.

Acknowledgments

This work was supported by Grant-in-Aid for Scientific Research (A) (No. 18206074) and Young Scientists (Start-up) (No. 20960049) from the Ministry of Education, Culture, Sports, Science and Technology (MEXT), Japan and in part by the Global COE (Center of Excellence) Program of International Center for Integrated Research and Advanced Education in Materials Science from the MEXT, Japan.

References

[1] Poutcharovsky DJ, Yvon K, Parthé E. J Less-Common Met 1975;40:139.

[2] Susz CP, Muller J, Yvon K, Parthé E. J Less-Common Met 1980;71:P1.

[3] Poutcharovsky DJ, Parthé E, Acta Cryst B 1974;30:2692.

[4] Gottlieb U, Sulpice A, Lambert-Andron B, Laborde O. J Alloys Compd 2003;361:13.

[5] Schwomma O, Preisinger A, Nowotny H, Wittman A. Monatsch Chem 1964;95:1527.

[6] Knott HW, Mueller MH, Heaton I. Acta Crystallogr 1967;23:549.

[7] Simkin BA, Hayashi Y, Inui H. Intermetallics 2005;13:1225.

[8] Ivanenko L, Filonov A, Shaposhnikov B, Behr G, Souptel D, Schumann J, Vinzelberg H, Plotnikov A, Borisenko V. Microelectronic Eng 2003;70:209.

[9] Souptel D, Behr G, Ivanenko L, Vinzelberg H, Shumann J. J Cryst Growth 2002;244:296.

[10] Zaitsev VK. Thermoelectric properties of anisotropic $MnSi_{1.75}$. In: Rowe DM, editor. CRC handbook on Thermoelectrics, New York (NY): CRC Press, 1994. p. 299.

[11] Nowotny H. In: Eyring L, O'Keefe M, editors. The chemistry of extended defects in non-metallic solids, Amsterdam: North-Holland, 1970. p. 223.

[12] Ye HQ, Amelinckx S. J Solid State Chem 1986;61:8.

[13] Simikin BA, Ishida A, Okamoto NL, Kishida K, Tanaka K, Inui H. Acta Mater 2006;54:2857.

[14] Jeitschko W, Parthé E. Acta Crsytallogr 1967;22:417.

[15] Frecrickson DC, Lee S, Hoffmann R, Lin J. Inorg Chem 2004;43:6151.

[16] Frecrickson DC, Lee S, Hoffmann R. Inorg Chem 2004;43:6159.

[17] Ishida A, Okamoto NL, Kishida K, Tanaka K, Inui H, Mater Res Soc Symp Proc 2007;980:II05-37.

[18] Kishida K, Ishida A, Koyama T, Harada S, Okamoto NL, Tanaka K, Inui H. Acta Mater 2009;57:2010-2019.

[19] Migas DB, Miglio L, Shaposhinikov VL, Borisenko VE. Phys Stat Sol 2002;231:171.

[20] Gröansson K, Engström I, Noläng B. J Alloys Compd 1995;219:107.

[21] de Ridder R, van Tendeloo G, Amelinckx S. Phys Stat Sol 1976;(a)33:383.

[22] Koyama T, Ishida A, Okamoto NL, Kishida K, Tanaka K, Inui H. [in preparation].

[23] Migas DB, Shaposhnikov VL, Filonov AB, Borisenko VE, Dorozhkin NN. Phy Rev B 2008;77:075205.

[24] Bhandari CM, Rowe DM, In: Rowe DM, editor. CRC handbook on Thermoelectrics, New York (NY): CRC Press, 1994. p. 43.

Table 1. Nominal compositions of the directionally solidified samples $Ru_{1-x}Mn_xSi_y$.

x	y
0.50	1.650
0.55	1.660
0.75	1.710
0.85	1.725
0.90	1.732

Figure captions

Fig. 1. (Color online) (a) Unit cell of Ru_2Si_3. (b) Projection of the unit cell of Ru_2Si_3 along the *c*-axis.

Fig. 2. (Color online) SEM-BEIs of as-arcmelted samples with nominal alloy compositions of (a)-(d) $Ru_{1-x}Mn_xSi_{1.5}$ and (f)-(i) $Ru_{1-x}Mn_xSi_{1.75}$ (x = 0.20, 0.40, 0.60, and 0.80). Below the BEIs are chemical compositions measured by SEM-EDS for (e) $Ru_{1-x}Mn_xSi_{1.5}$ and (j) $Ru_{1-x}Mn_xSi_{1.75}$ alloys.

Fig. 3. (Color online) Powder x-ray diffraction patterns from $Ru_{1-x}Mn_xSi_{1.5}$ alloys with x = 0.05, 0.20, 0.40, 0.60, and 0.80.

Fig. 4. Compositional dependence of (a) the lattice constants and (b) the cell volume of the M subcell of the chimney-ladder phase in $Ru_{1-x}Mn_xSi_{1.5}$ alloys with x = 0.05, 0.20, 0.40, 0.60, and 0.80 and Mn_4Si_7 [21].

Fig. 5. (a) Microstructure of a $Ru_{1-x}Mn_xSi_{1.75}$ alloy with x = 0.60 and (b)-(d) SAED patterns of the $[120]_M$ incidence taken from the regions marked ‘b’, ‘c’ and ‘d’ in (a).

Fig. 6. Variation of the 00*l* systematic rows of SAED patterns of the $[120]_M$ incidence. The Mn/M, c_{Si}/c_M and Si/M ratios determined by TEM-EDS analysis and Eqs. (1) and (2) are also indicated.

Fig. 7. Si/M ratios of the chimney-ladder phases in the Ru-Mn-Si system (Ru-Re-Si) plotted against the Mn (Re) content [13].

Fig. 8. Phase relationships among silicon, $(Ru,Mn)Si_y$ sesquisilicide and (Ru,Mn)Si monosilicide phases.

Fig. 9. (Color online) SEM-BEIs and compositional distributions of directionally solidified alloys with nominal compositions of $Ru_{1-x}Mn_xSi_y$ (x = 0.50, 0.55, 0.75,

0.85 and 0.90).

Fig. 10. (Color online) Temperature dependence of thermoelectric properties of directionally solidified alloys $Ru_{1-x}Mn_xSi_y$. (a) Seebeck coefficient, (b) electrical resistivity, (c) thermal conductivity, (d) power factor and (e) dimensionless figure of merit (ZT). The highest values of power factor and ZT obtained among the Ru-Re-Si chimney-ladder compounds are also indicated in (d) and (e), respectively [18].

Fig. 11. (a) VEC values per M atom for the $Ru_{1-x}Mn_xSi_y$ chimney-ladder phases plotted against the Mn content. (b) Atomic packing factors of the $Ru_{1-x}Mn_xSi_{1.5}$ samples (x = 0.20, 0.40, 0.60, and 0.80) and Mn_4Si_7 [21].

Fig1

Click here to download high resolution image

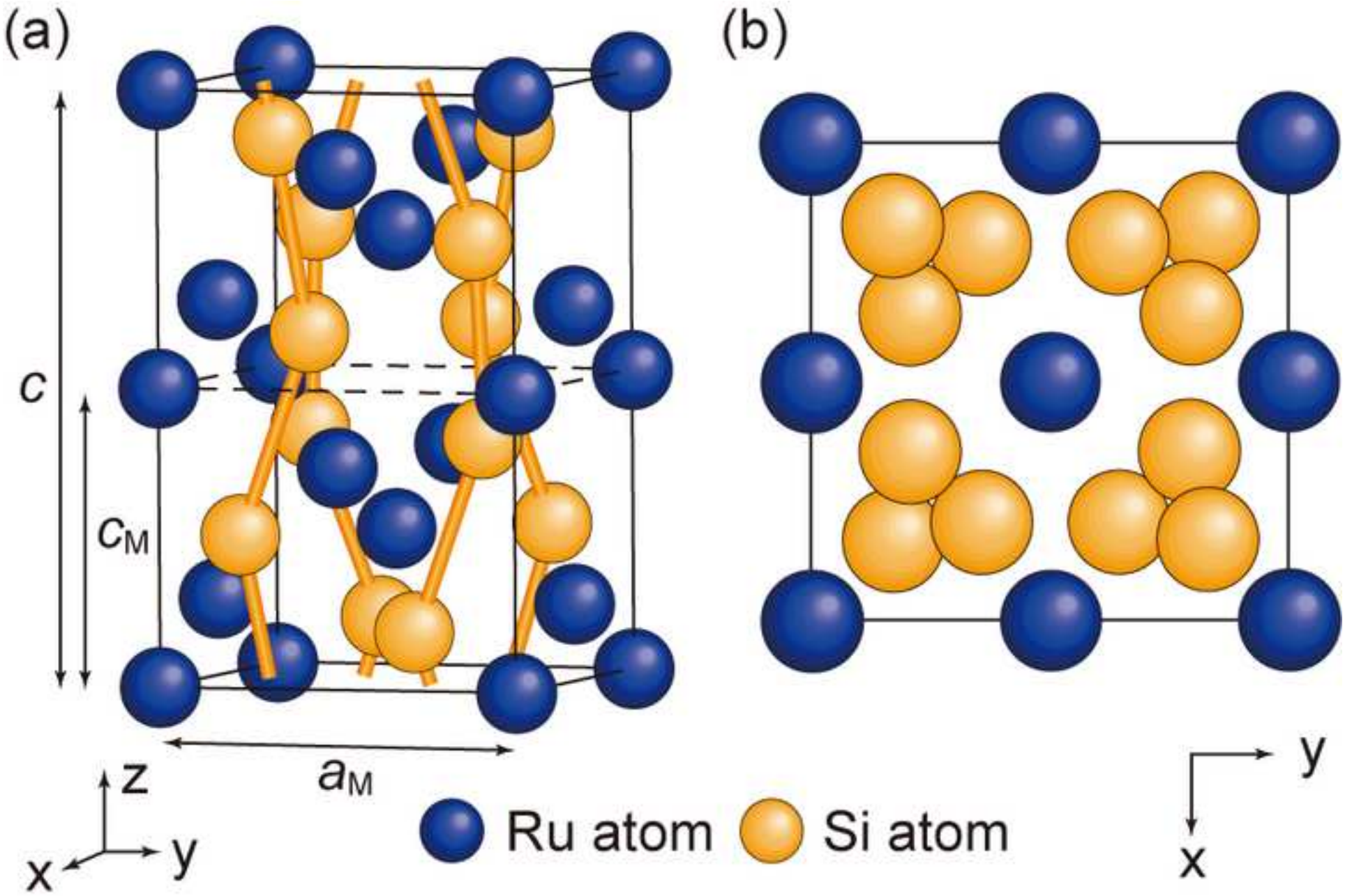

Fig2

Click here to download high resolution image

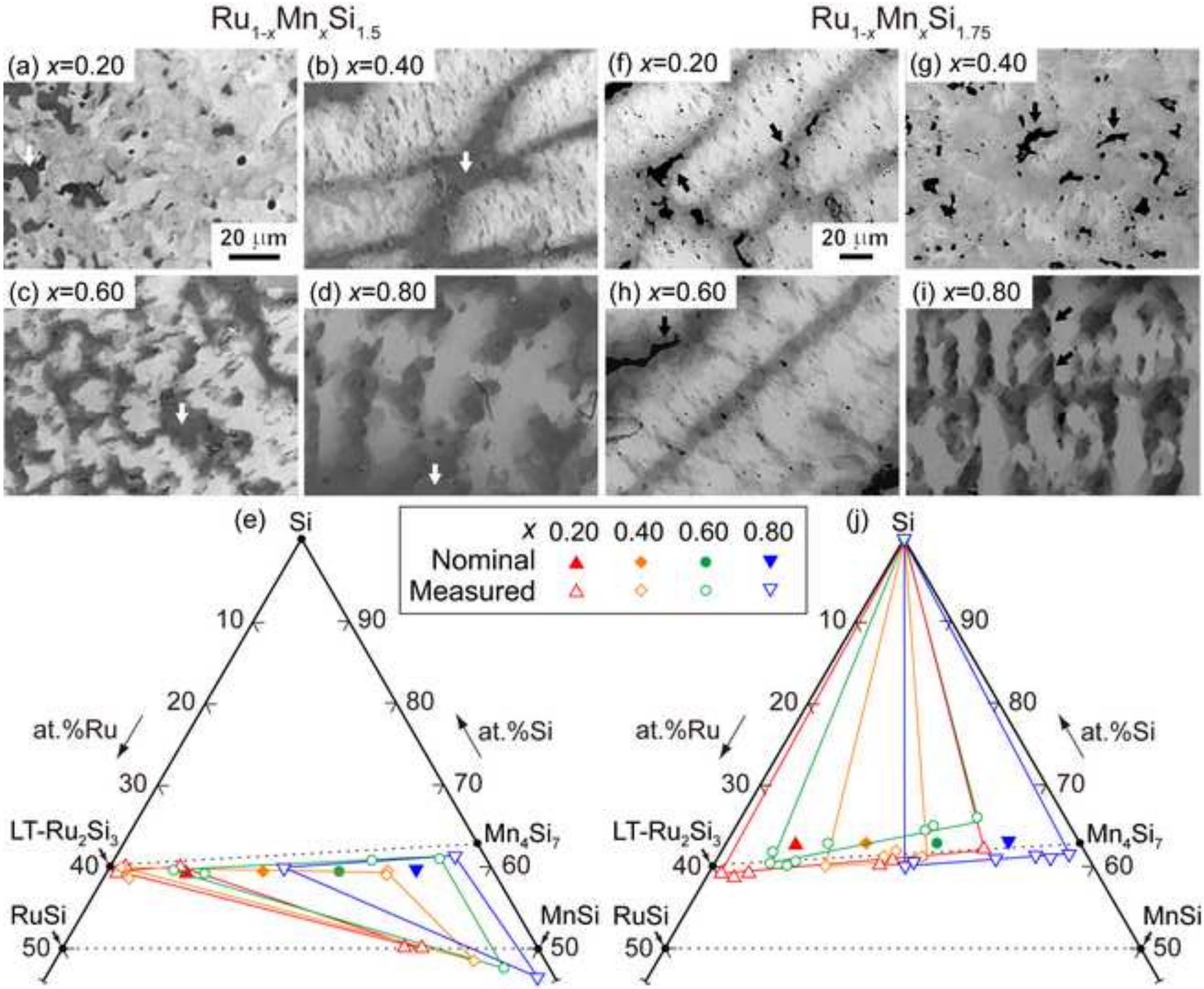

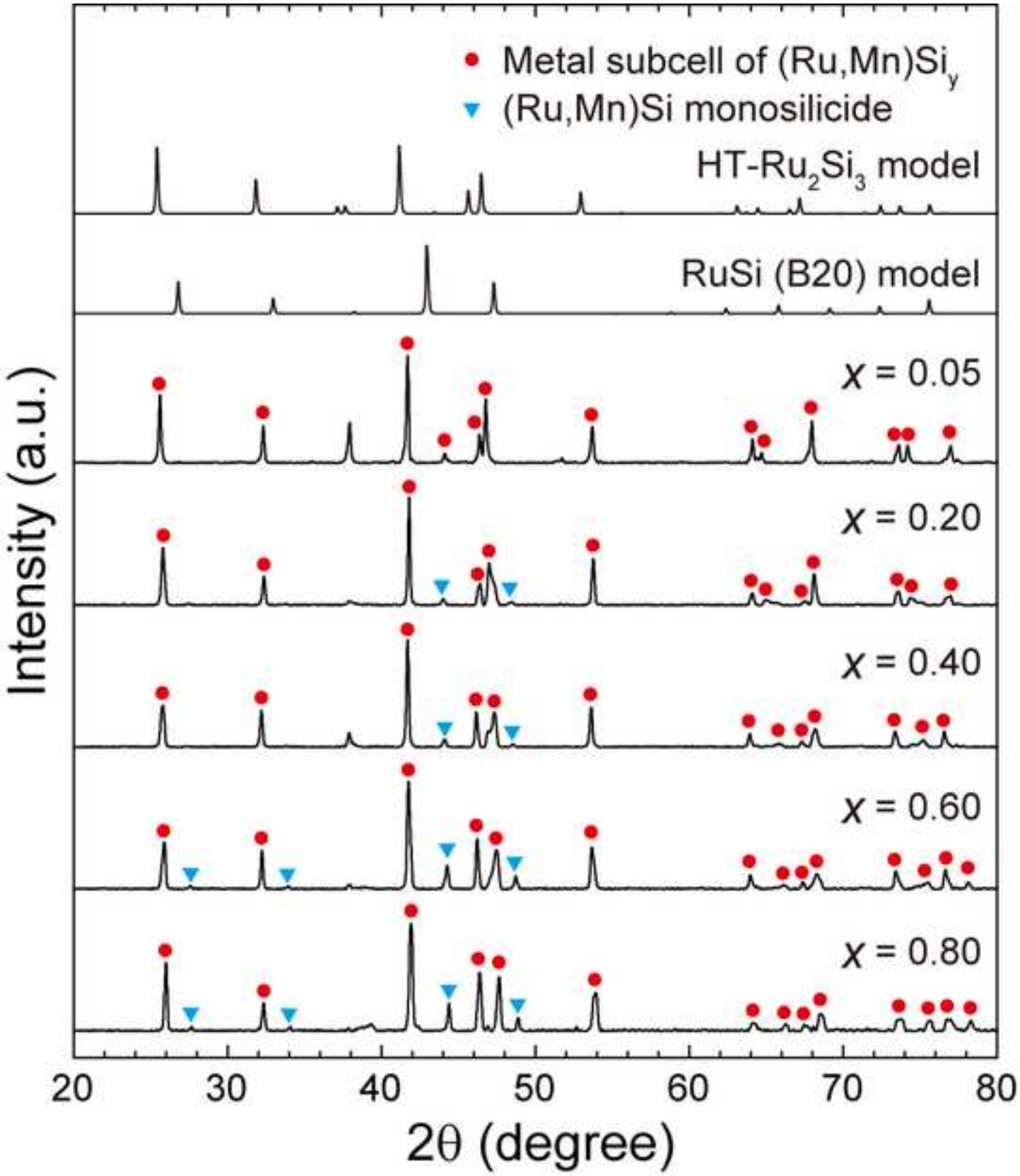

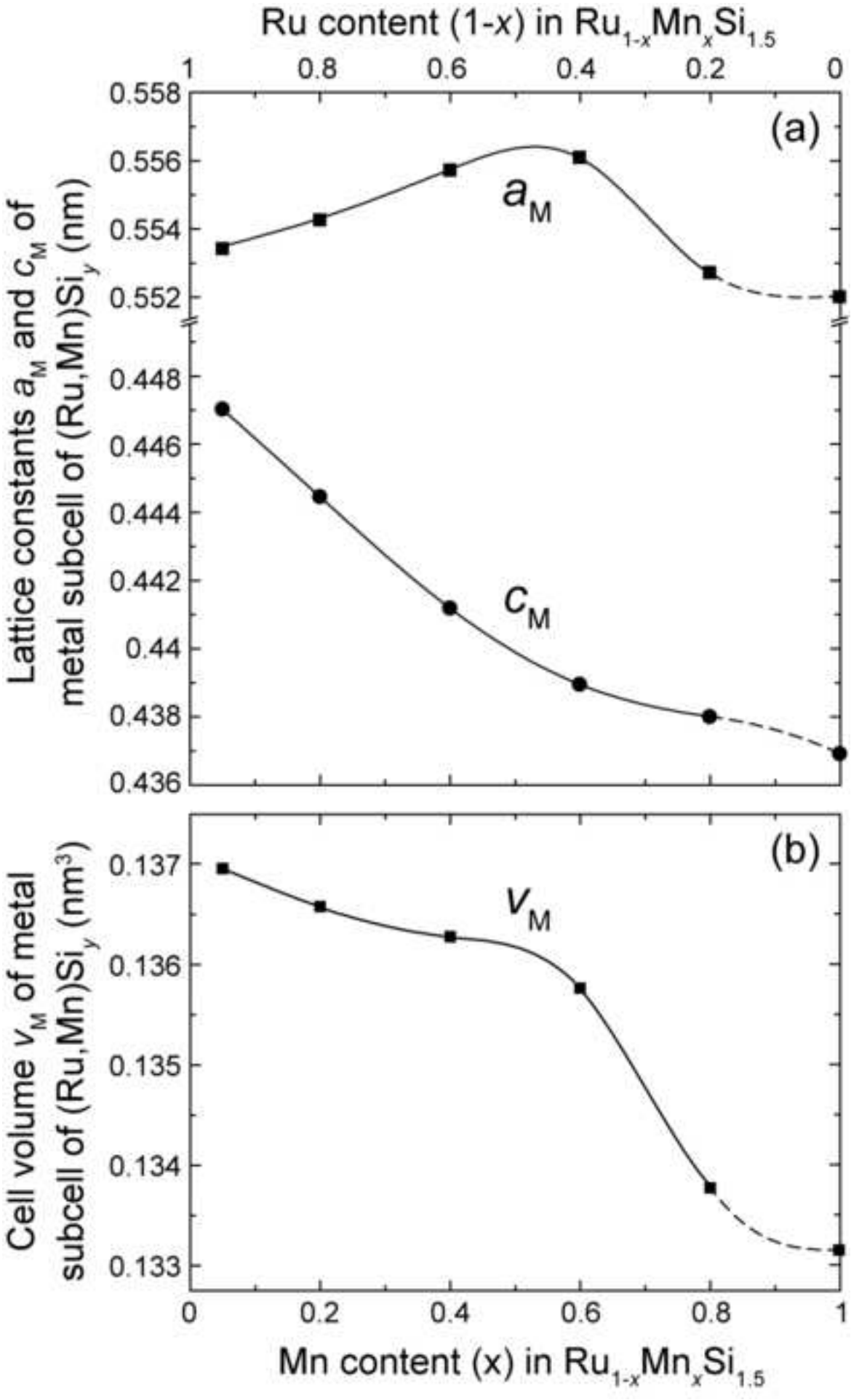

Fig5

Click here to download high resolution image

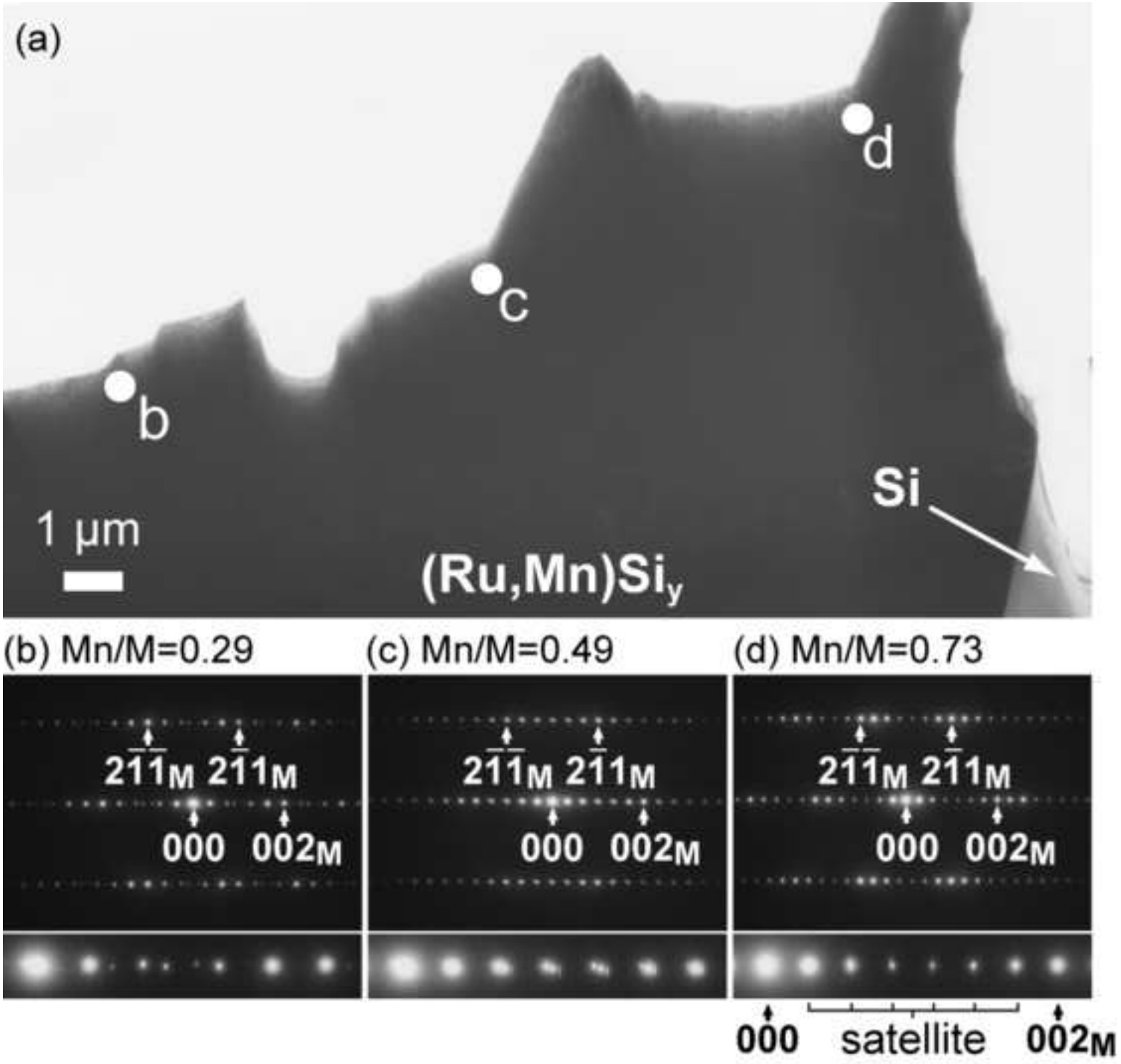

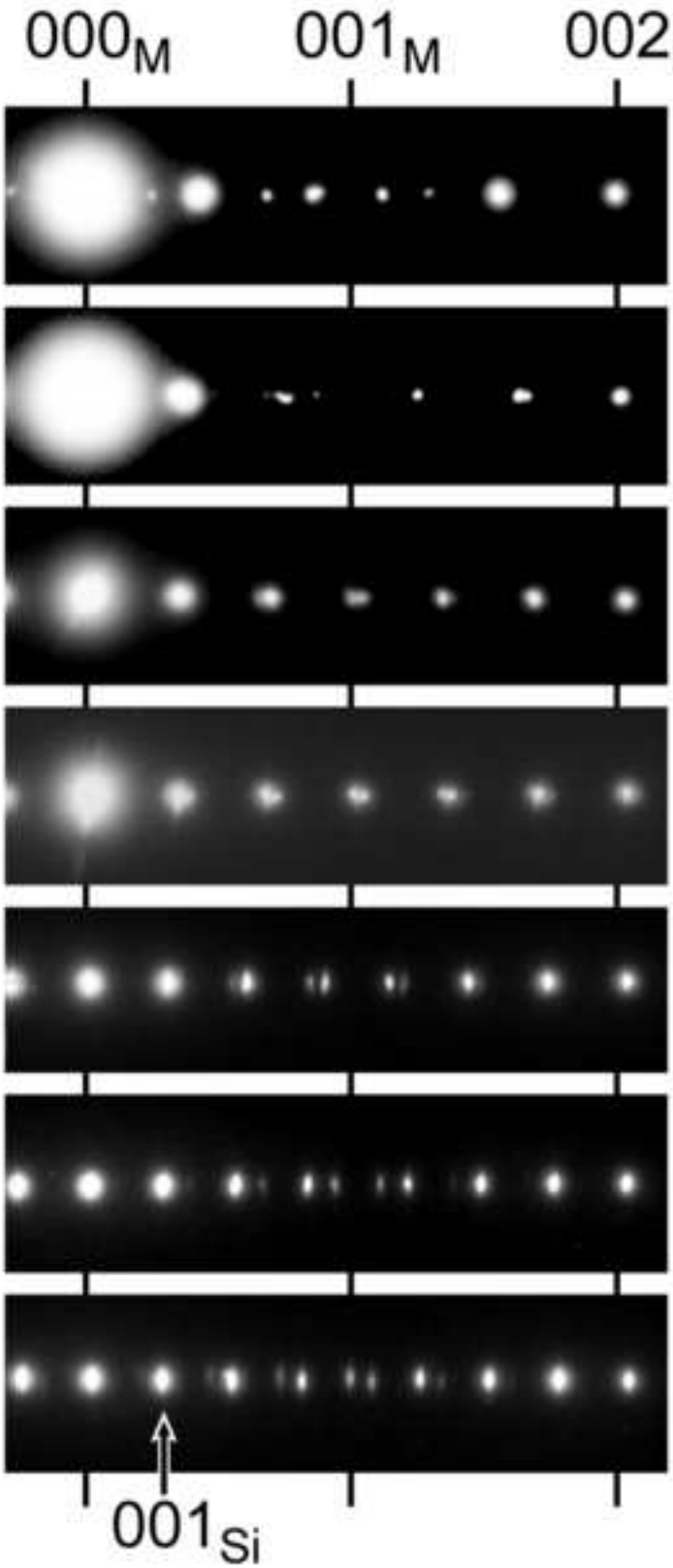

	Mn/M (%)	c_{Si}/c_M	Si/M
(a)	12.9	2.288	1.563
(b)	27.9	2.639	1.621
(c)	37.3	2.941	1.660
(d)	50.0	3.003	1.667
(e)	71.9	3.401	1.706
(f)	88.6	3.676	1.728
(g)	93.0	3.846	1.740

Fig7

Click here to download high resolution image

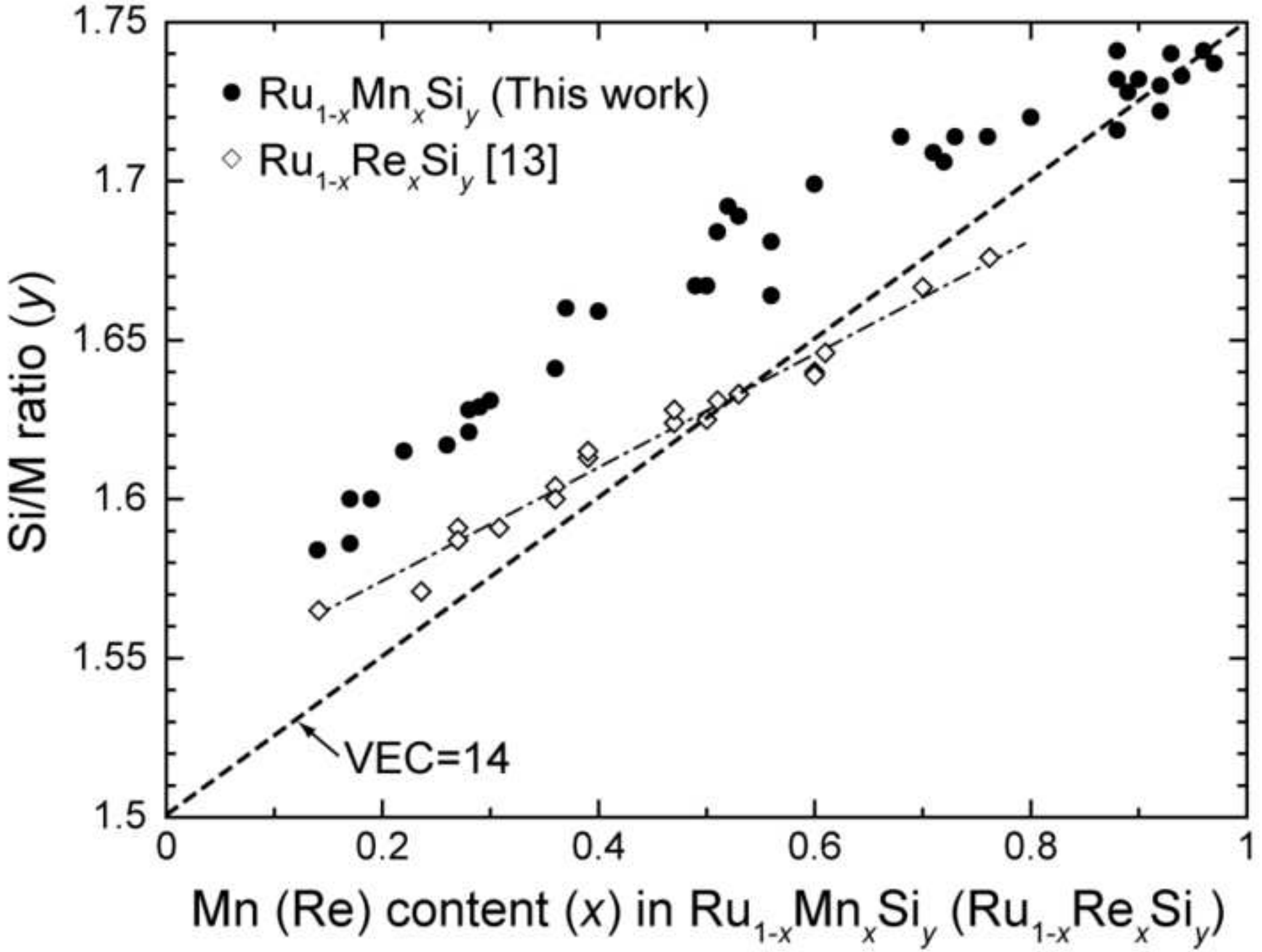

Fig8

Click here to download high resolution image

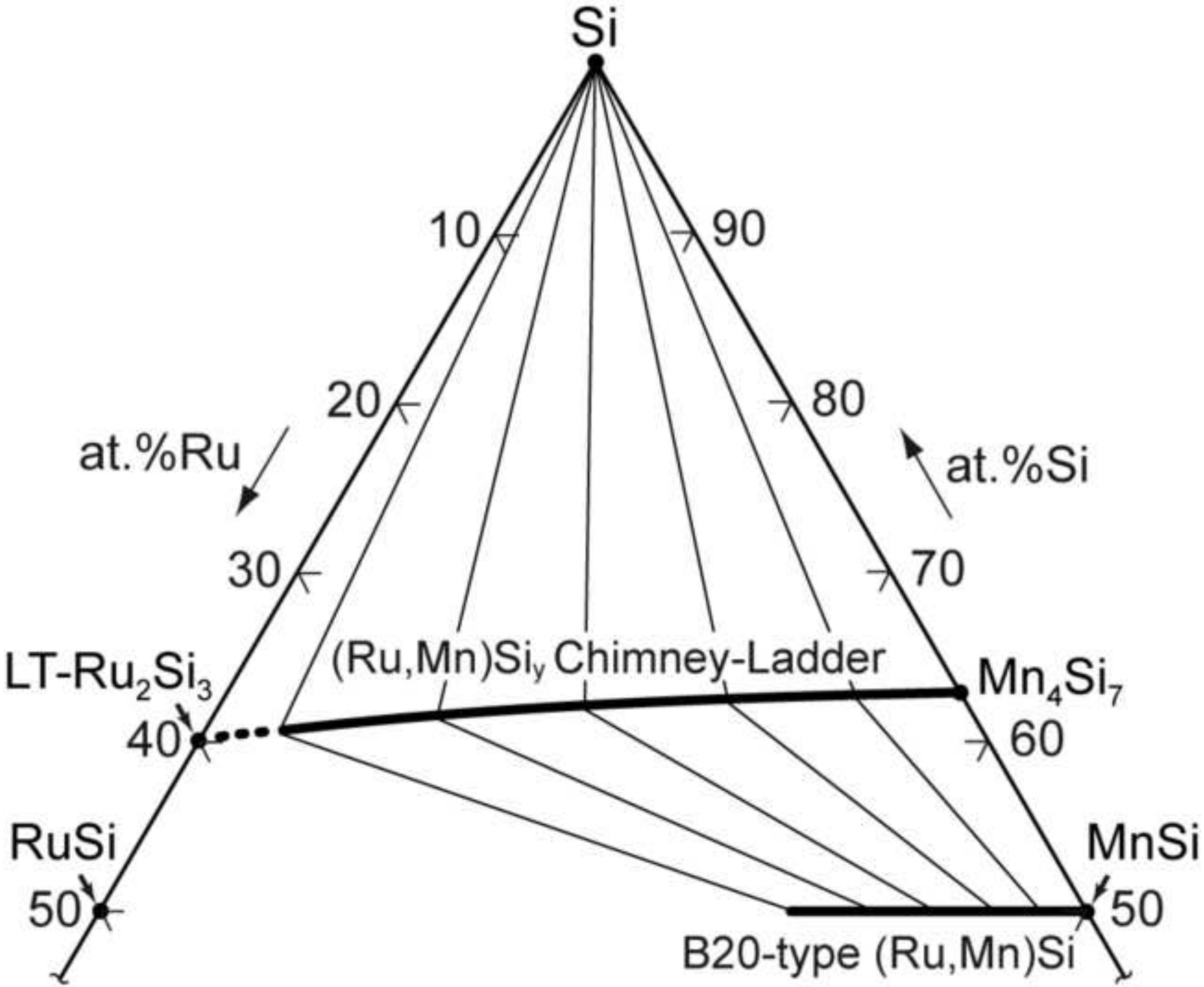

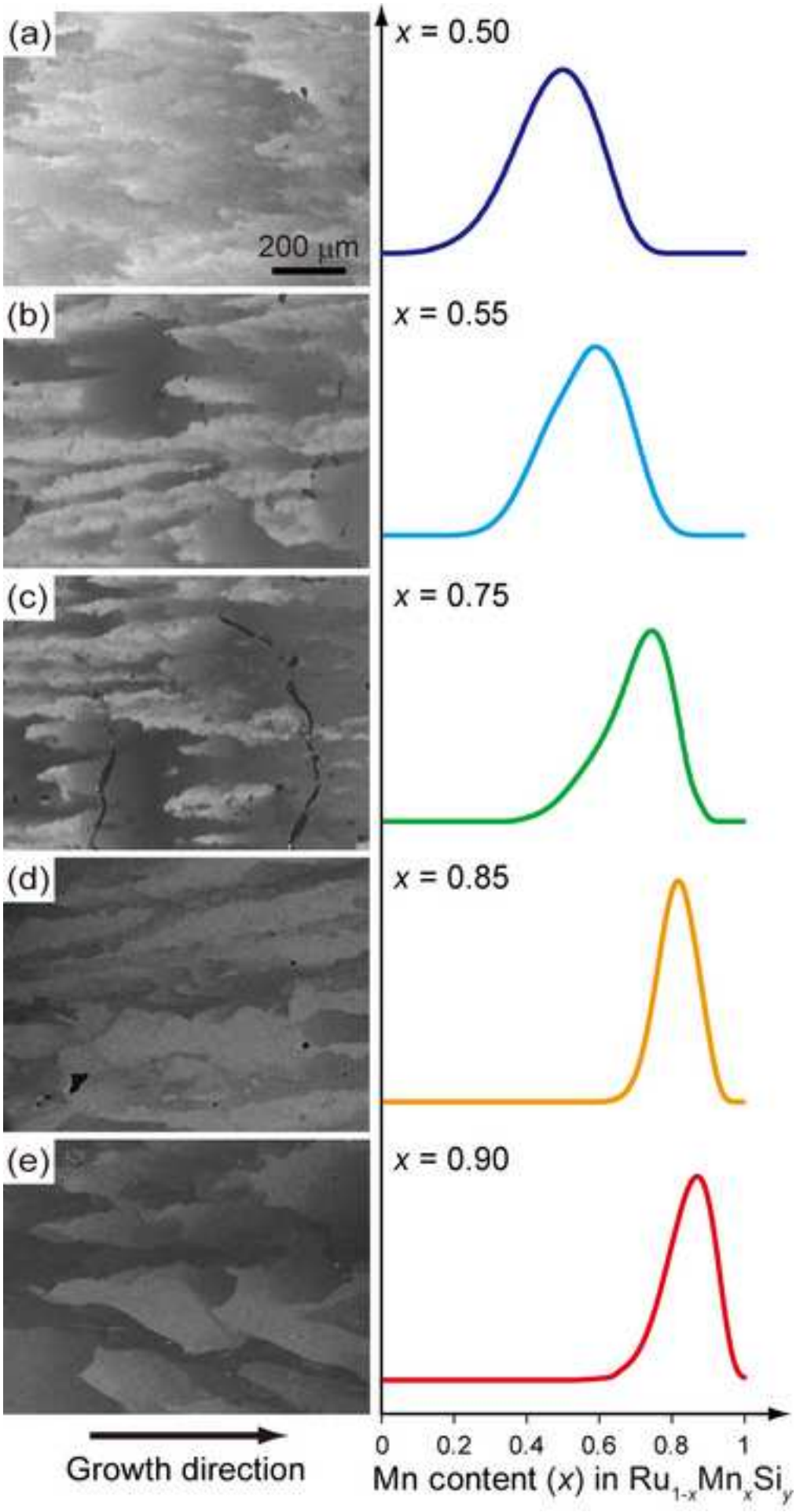

Fig10

Click here to download high resolution image